PROJECTED STRUCTURE OF THE PORE-FORMING OmpC PROTEIN FROM *ESCHERICHIA COLI* OUTER MEMBRANE

CHUNG-FU CHANG,* SHOJI MIZUSHIMA,‡ AND ROBERT M. GLAESER§
**Pennsylvania Muscle Institute, University of Pennsylvania School of Medicine, Philadelphia, Pennsylvania 19104; ‡Laboratory of Microbiology, Faculty of Agriculture, Nagoya University, Chikusa, Nagoya 464, Japan; and §Department of Biophysics and Medical Physics, Donner Laboratory, University of California, Berkeley, California 94720*

ABSTRACT A single-projection structure analysis of a bacterial outer membrane protein, OmpC, has been carried out by electron microscopy of frozen hydrated specimens. Two distinct crystal polymorphs have been observed in the frozen-hydrated samples, and projection structures of both forms have been obtained to a resolution of 13.5 Å. Preliminary examination of negatively stained samples revealed the expected, trimeric appearance of pores in the OmpC specimens. Electron microscopy of unstained, frozen-hydrated OmpC reveals the trimeric pore structure with equal clarity. In addition, the overall molecular envelope of the protein is readily discerned, and a major lipid-containing domain can also be seen. Because of the small coherent patch size, mosaic disorder, and unpredictable polymorphism of the presently available specimens, three-dimensional reconstruction of frozen-hydrated OmpC has not been carried out.

INTRODUCTION

The outer membrane of *Escherichia coli (E. coli)*, like that of other gram negative bacteria, contains a small variety of pore-forming proteins, which can occur in quite large quantities. Two of these outer membrane proteins (~36,500 mol wt), referred to as OmpC and OmpF, respectively, are known to serve as transmembrane channels of rather large pore diameter (Schindler and Rosenbusch, 1978; Nikaido and Rosenberg, 1983), which permit the nonspecific, passive diffusion of small (<660 mol wt), water-soluble solutes into and out of the periplasmic space (Nakae, 1976). Under conditions of normal laboratory culture, OmpF is the predominant pore-forming protein that is present in the outer membrane (Steven et al., 1977), but OmpF is replaced by OmpC in cells that have been grown under conditions of high osmotic stress (Kawaji et al., 1979; van Alphen and Lugtenberg, 1977). OmpF and OmpC can be solubilized as protein trimers, which can be reconstituted in a functional form either in lipid vesicles (Yamada and Mizushima, 1978) or in black lipid films (Schindler and Rosenbusch, 1981). In the latter case, electrical measurements have demonstrated that OmpF pores exist in an open and a closed state, and that the opening and closing of individual pores within a trimer is a highly cooperative event.

The characterization of OmpF structure has included spectroscopy (Rosenbusch, 1974; Nakamura et al., 1974), electron microscopy (Steven et al., 1977; Dorset et al., 1983), and x-ray diffraction studies (Garavito et al., 1983), as well as the complete determination of the primary amino acid sequence (Chen et al., 1982) and the corresponding nucleotide sequence (Inokuchi et al., 1982) of the protein. The spectroscopic data reveal a high percentage of β-sheet secondary structure with no detectable amount of α-helix. The trimeric structure of aqueous channels is clearly depicted in electron micrographs of negatively stained samples (Steven et al., 1977; Dorset et al., 1983). Three-dimensional image reconstruction of negatively stained OmpF trimers, reconstituted in phospholipid, reveals the unexpected merging of three distinct channels from one side of the membrane into a single channel on the other side (Dorset et al., 1984). Electron microscopy of negatively stained samples gives little indication, however, of the distribution of protein within the unit cell. Very well-ordered three-dimensional crystals of detergent-solubilized OmpF trimers have been grown (Garavito et al., 1983), but x-ray crystallographic structure analysis has not yet advanced to the stage where retrieving phase values by multiple isomorphous replacement has been possible.

Here we present results of a structure analysis in projection, by electron microscopy, of specimens of OmpC that have been prepared by reconstitution with lipid A, the core portion of outer membrane lipopolysaccharide. Yamada and Mizushima (1980) have shown that OmpC specimens thus prepared are in a two-dimensional crystalline form. Examination of negatively stained samples verifies, as expected, that the trimeric appearance of pores in the OmpC samples is very similar to that observed in OmpF. Electron microscopy of unstained, frozen hydrated specimens also reveals the trimeric pore in OmpC specimens with equal clarity; in addition, the overall molecular

envelope is readily discerned. A major lipid-containing domain can be seen that is capable of accommodating two moles of lipid A per mole of OmpC. Two distinctly different crystal polymorphs have been observed in the frozen hydrated samples, and projection structures of both forms have been obtained to a resolution of 13.5 Å. Because of the small coherent patch size, mosaic disorder and unpredictable polymorphism of the presently available specimens, three-dimensional reconstruction of OmpC in the frozen hydrated state will be difficult and must await methods for producing larger and better-ordered crystals.

MATERIALS AND METHODS

Samples of OmpC protein were isolated from the outer membranes of a mutant strain of *E. coli* K-12 identified as *E. coli* YA21 (K-12, F^- met leu λ^-). Procedures for bacterial growth and protein isolation were as described by Yamada and Mizushima (1980). Lipid A was prepared from lipopolysaccharide of YA21 by acetic acid hydrolysis as described by Galanos et al. (1971). Solubilized, trimeric OmpC was reconstituted with lipid A as described by Yamada and Mizushima (1980). Briefly, purified OmpC, 400 μg, was incubated for 30 min with 0.5 M NaCl in 100 μl of 100 mM Tris-HCl (pH 8.0), 1% sodium dodecylsulfate (SDS), and 0.1% 2-mercaptoethanol at 37°C. The solution was then mixed with 60 μg of lipid A (~1,500 mol wt) in 100 μl of 1% SDS. The mixture was dialyzed against 5 mM $MgCl_2$, 10 mM Tris-HCl (pH 8.0), 0.025% 2-mercaptoethanol at 25°C for 48 h. The resulting precipitate, consisting of reconstituted vesicles with ordered arrays, was washed by centrifugation and stored in distilled water with 0.02% sodium azide.

Uranyl formate, prepared at a concentration sufficient to give an absorbance value of 0.09 at 450 nm (Williams, 1981), was used in making negatively stained specimens. No special precautions were taken to limit the electron exposures used when imaging negatively stained samples.

Unstained frozen hydrated specimens were prepared by a modification of the stearic acid monolayer technique (Hayward et al., 1978). Behenic acid, CH_3 $(CH_2)_{20}$ COOH, was used rather than stearic acid, so that distilled water (rather than 5 mM $CaCl_2$ solution at a pH 8.0) could be used in the subphase (Chang et al., 1984). In addition, the polylysine solution, which is used to render the support film hydrophilic, was applied a second time after adsorption of the specimen material to the support film in order to facilitate adhesion of the behenic acid monolayer. Individual electron microscope grids were frozen by manual insertion directly into liquid nitrogen.

Electron microscopy was carried out on a high resolution cold stage (Hayward and Glaeser, 1980), which was maintained at a stage temperature of approximately −125°C. Images used for high resolution work were recorded at a magnification of 31,500, with an electron exposure of ~5 electrons/Å^2. The objective lens was underfocused with a value of ≤2,000 Å. Specimens were scanned beforehand at very low magnification, at a dose rate of 1 electron/Å^2 per minute in order to select areas where the reconstituted membranes could be seen to be only a single layer in thickness.

Areas of electron micrographs that were suitable for image processing were first identified by optical diffraction, after which the negatives were scanned and digitized with a Perkin-Elmer PDS scanning microdensitometer (Perkin-Elmer Corp., Instrument Div., Norwalk, CT). When digitizing high resolution images of frozen hydrated specimens, a spot size (and sampling distance) of 10 μm was used, corresponding to ~3.2 Å at the specimen. Image processing was performed with computer programs developed for the VAX 11/780 system (Digital Equipment Corp., Marlboro, MA) primarily by Dr. David A. Grano. Fourier transforms were generally calculated for an array of 512 by 512 image points. A reciprocal lattice was defined by seeking a least-square best fit to selected, strong peaks in the Fourier transform, and values of the amplitude and phase of the Fourier transform at all lattice positions were then printed out as 9 × 9 arrays centered about each point of the lattice. When necessary, the reciprocal lattice was further refined, using new peak positions observed in the 9 × 9 display. An example of the type of result obtained is illustrated in Table I. The circled numbers in each amplitude array box are the diffraction peaks. The phase values associated with the circled amplitudes have not yet been referred to a crystallographic symmetry origin.

In our present studies we have obtained two types of data sets, referred to as Type I and Type II. To compare the two data sets, the Fourier transforms were indexed in a mutually consistent fashion, such that the aqueous channels and a second major negative domain would be superimposed in the respective images.

RESULTS

The majority of the reconstituted membranes obtained by the current specimen-preparation method have the appearance of closed vesicles (shown in Fig. 1), which have been collapsed or flattened onto the support film. Occasionally, membrane sheets are found that have the appearance of torn or ruptured vesicles, and that are only a single layer in thickness. Although the reconstituted vesicles (and sheets) tend to be between 0.5 and 1.0 μm in diameter, the crystalline domains within the plane of the membrane show considerable mosaicity, and the size of individual coherent domains has been found to be only 500 to 1,000 Å.

A typical negatively stained sample was first selected for image processing in order to make a comparison with published studies of OmpF. Fig. 2 shows the original micrograph, which is of an area where two membrane sheets have collapsed, face-to-face, in a crystallograhically ordered bilayer. Crystallographic ordering of the two layers is demonstrated by the fact that the filtered image (Fig. 4 *a*), like those published of OmpF specimens (Dorset et al., 1983), shows an otherwise unexpected line of nearly perfect mirror symmetry along the center-to-center axis between trimers. Three-dimensional reconstruction of such specimens confirms further the crystallographic ordering of the two layers in a face-to-face orientation (Dorset et al., 1984). The filtered image of the negatively stained OmpC sample is very similar to images of OmpF; the major structural feature is the intensely stained trimer of pores (Grano et al., 1982), with a very weak stain-excluding domain that is nested within the groove or indentation between two pores in the trimer.

The negatively stained specimen in Fig. 2 provides a good illustration of the mosaic domain structure and limited degree of coherent ordering that is present in the membrane sheets. Crystalline defects in the specimen are best visualized by viewing the micrograph at a steeply inclined angle, so as to sight along the lattice rows. The considerable disorder that then becomes evident is apparently not an artifact of negative staining or of the face-to-face association of two membrane sheets; as shown below, similar evidence of mosaicity and disorder is exhibited in optical diffraction patterns of frozen hydrated single layers.

Low-dose images of frozen hydrated OmpC specimens, recorded with a total electron exposure of ~5 electrons/Å^2, show no discernable image detail, due to their inherently low contrast and the poor degree of statistical definition. However, the existence of a periodic lattice in these images is readily seen in optical diffraction patterns obtained with such images. In particular, strong (2, 1) reflections are visible in specimen areas of the best quality.

Two types of optical diffraction pattern have been observed from frozen hydrated images of specimens that are only a single layer thick. In the first type, a relatively complete reciprocal lattice is unambiguously seen, consisting of the (1, 1), (2, 0), (1, 2), and (2 ,1) reflections. An example of such a pattern, referred to as a Type I pattern, is shown in Fig. 3 *a*. The other type of pattern, referred to as a Type II pattern, consists of only the (2, 1) reflection, all of the lower resolution spots being too weak to detect by optical diffraction. An example of such a pattern is seen in Fig. 3 *b*. These two types of pattern seem to reflect the presence of two legitimately different structural states,

TABLE I
REPRESENTATIVE COMPUTER OUTPUT OF A PORTION OF THE FOURIER TRANSFORM

$H = 2$ $K = 1$
Location of largest peak in block = (210, 303)
Scale = 0.1E–02 Middle = (210, 303)

	Amplitudes									Phases								
R C	299	300	301	302	303	304	305	306	307	299	300	301	302	303	304	305	306	307
206	10	8	28	13	27	28	11	5	14	234	336	138	206	14	335	115	234	233
207	32	18	17	22	41	20	23	13	19	85	22	334	169	215	144	167	291	303
208	17	5	12	26	12	44	20	17	28	327	170	334	323	21	300	118	243	332
209	5	41	7	42	33	13	9	21	18	232	97	350	46	218	3	282	210	224
210	19	11	51	56	(105)	66	19	23	37	191	257	35	160	260	245	113	338	302
211	4	15	10	8	26	39	31	31	7	183	323	146	220	87	234	356	56	180
212	28	12	30	21	6	7	19	14	10	131	349	249	3	265	158	298	112	130
213	16	11	30	11	21	11	21	31	17	172	130	276	87	344	43	117	243	247
214	32	17	32	13	10	30	4	19	5	155	90	257	157	132	301	264	37	162

$H = -3$ $K = 2$
Location of largest peak in block = (240, 192)
Scale = 0.1E–02 Middle = (241, 192)

	Amplitudes									Phases								
R C	188	189	190	191	192	193	194	195	196	188	189	190	191	192	193	194	195	196
237	21	8	19	32	28	27	26	27	8	188	268	78	107	341	352	142	49	24
238	9	21	16	17	28	41	14	23	12	137	149	233	329	358	83	10	188	260
239	23	26	17	35	13	22	17	8	17	170	259	136	109	325	346	162	315	299
240	13	13	21	43	(102)	23	13	21	12	298	270	360	45	76	29	102	310	65
241	12	23	15	40	98	28	37	22	2	276	10	356	64	90	247	358	263	157
242	5	24	32	9	28	24	22	21	31	64	57	209	26	22	318	138	345	65
243	12	10	15	6	23	25	15	26	21	97	336	239	50	254	126	281	244	211
244	18	16	15	39	19	15	30	7	15	59	233	183	262	203	151	185	32	268
245	26	14	25	15	17	27	15	15	5	230	25	3	104	99	62	336	176	91

$H = 1$ $K = -3$
Location of largest peak in block = (321, 276)
Scale = 0.1E–02 Middle = (321, 276)

	Amplitudes									Phases								
R C	272	273	274	275	276	277	278	279	280	272	273	274	275	276	277	278	279	280
317	10	18	22	5	6	1	36	35	15	24	136	251	320	143	82	117	228	64
318	29	14	17	30	10	15	6	19	22	260	170	224	43	164	30	277	45	34
319	21	24	23	21	15	18	18	17	13	133	311	120	358	111	99	185	327	58
320	17	2	16	10	58	56	5	25	15	271	64	73	270	36	101	248	259	329
321	29	7	17	39	(102)	40	10	6	12	360	122	319	139	62	147	159	83	75
322	29	35	12	42	30	2	18	4	8	307	26	230	179	360	175	75	131	218
323	11	14	24	21	13	9	35	29	6	238	169	112	177	256	83	14	120	211
324	52	19	8	27	49	21	19	12	18	19	57	94	316	237	165	161	282	123
325	5	17	17	10	23	15	1	6	15	325	184	137	208	9	37	52	291	258

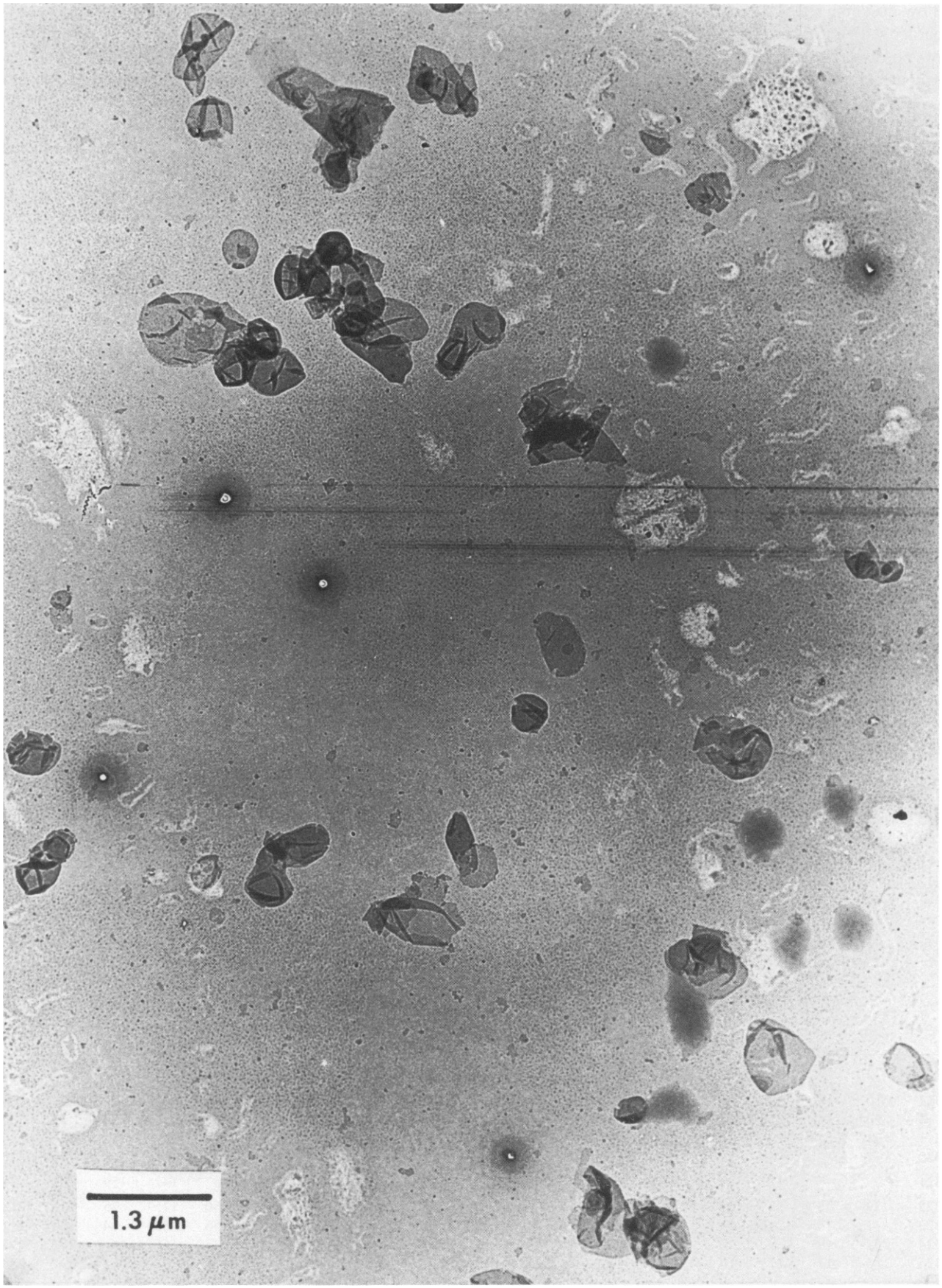

FIGURE 1 Low magnification image of an OmpC specimen that was prepared with the behenic-acid monolayer technique. The image was recorded at room temperature and the specimen was air dried.

rather than differences in the electron microscope imaging conditions, since they can be recorded from adjacent areas on the same micrograph, separated by a distance as small as 0.5 μm at the specimen.

Values of the amplitude and phase obtained for symmetry related reflections are presented in Table II for the highest resolution data set obtained for a Type I image and for a similar high resolution data set of Type II. The column labeled amplitude represents the largest amplitude value found within a 9 × 9 box, subject to the further condition that it must be found within ±1 element of the position of the reciprocal lattice point generated by the least-squares fitting procedure. The column labeled phase is the phase at the same point as the peak amplitude. The values of the phase have all been referred at this point to a common threefold symmetry axis. The mean value and the standard deviation of values within the 9 × 9 box, excluding a 3 × 3 array centered at the expected lattice point, have also been calculated. These values have been used to compute the value of the peak minus the background, expressed in units of the standard deviation of the background.

The reliability of high resolution phase information for both data sets was estimated in terms of the figure of merit value (Hayward and Stroud, 1981), which has been routinely used for error analysis in x-ray crystallography

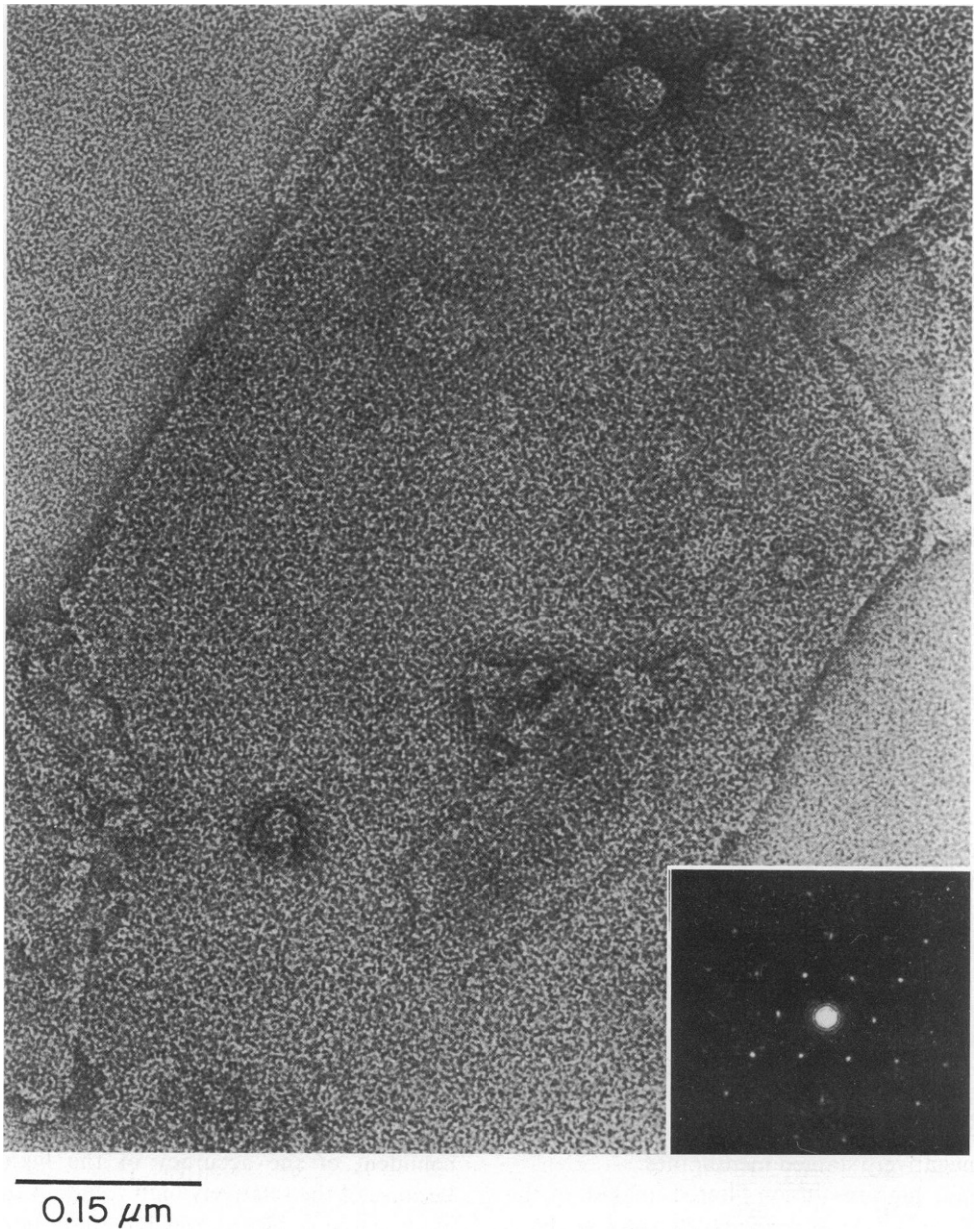

FIGURE 2 Image of OmpC specimens negatively stained with uranyl formate. The optical diffraction pattern of this image is shown (*lower right*). The highest reflection order visible is the (2,1).

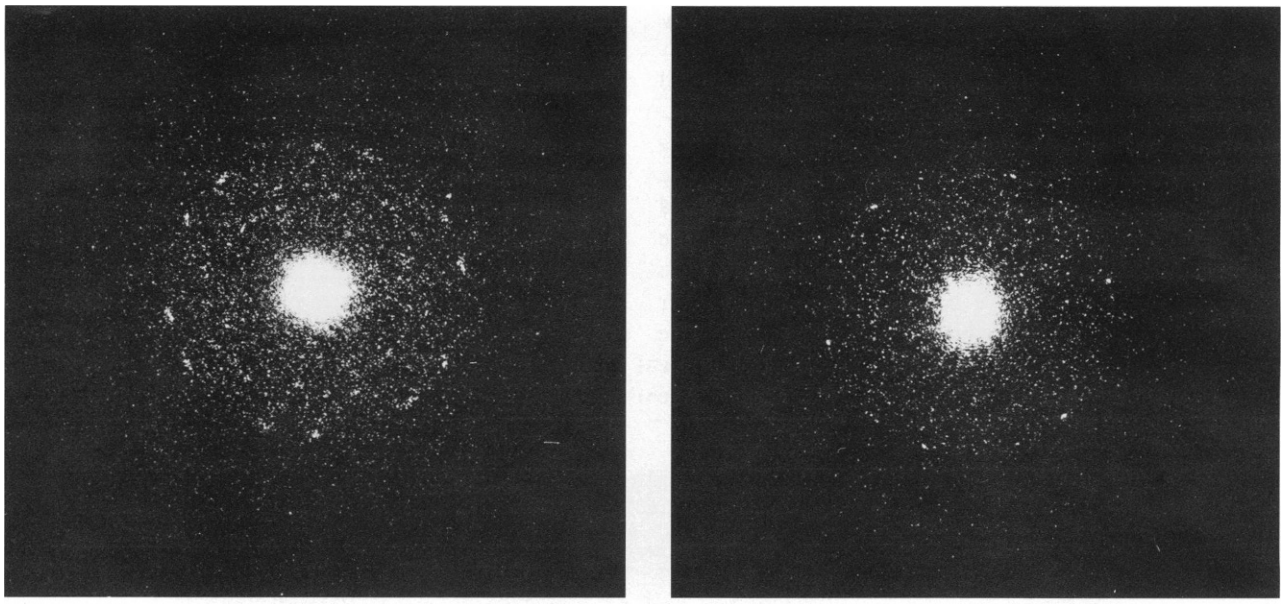

FIGURE 3 Optical diffraction patterns of OmpC specimens that were located on the same micrograph, separated by 0.5 μm. (*a*) Type I pattern shows a full reciprocal lattice consisting of the (1,1), (2,0), (1,2), and (2,1) reflection orders. (*b*) Type II pattern consists of only the (2,1) reflection, all of the lower resolution spots being too weak to detect by optical diffraction.

(Blow and Crick, 1959). The figure of merit (*m*) associated with each reflection order is shown in Table II.

To compare filtered images of the frozen hydrated specimens to images of the negatively stained specimen, all at the same resolution, inverse Fourier transforms that include symmetrized Fourier coefficients up to the (1, 2) and (2, 1) reflections are presented in Fig. 4. The triplet pore is readily identified as the strongly negative trimeric feature in the images of both types of frozen hydrated specimen. While the pore in frozen hydrated specimens is very similar to that seen in the negatively stained sample, the projected image of the pores is no longer aligned as precisely on a mirror symmetry line as it is in the negatively stained double layer. Major features of the shape, or molecular envelope, of the protein are now readily seen as positively contoured regions in both types of frozen hydrated specimen. In addition, a second major negative domain is revealed at one of the other threefold axes in the images of frozen hydrated specimens. We have found that the basic similarity between the filtered image of the negatively stained specimen and the filtered images of the frozen hydrated specimens can be artificially enhanced if the (1, 0) reflection is omitted from the Fourier synthesis of the negatively stained specimen. The (1, 0) reflection is actually too weak to observe in frozen hydrated specimens but is strong in negatively stained membranes.

Figs. 5 *a, b* show high resolution filtered images, of the Type I and the Type II data, respectively, which have been synthesized from the Fourier coefficients shown in Table II. For each triplet, the amplitudes and phases from Table II were used to calculate the weighted amplitude, the composite phase, and the joint figure of merit. The calculations were carried out as described by Downing and Glaeser (1984). The final values of weighted amplitude, composite phase, and composite figure of merit are shown in Table III. The highest reflection order incorporated in both images corresponds to a resolution of 13.5 Å. All the filtered images have the same contour interval and the same contour representation; the positive contours (solid lines) represent the high density domain and the negative contours (dotted lines) represent the low density one. Fig. 5 *a, b* show the readily identified triplet pore as a strongly negatively trimeric feature. The positively contoured regions, which represent the molecular shape of the protein, are also readily identified. In addition, a second major negative domain also exists in Fig. 5 *a, b*.

The difference in the structure factors for the Type I and Type II images are very substantial as can be seen most easily by inspection of the symmetrized data in Table III. In addition to the strikingly large value of the (2, 1) reflection in the Type II structure, which was first seen in the optical diffraction pattern, one can now see that the phases of equivalent reflections are often quite dissimilar, and many of the higher resolution spots have statistically reliable values in only one image but not the other. We are confident of the accuracy of the high resolution data because of the relatively high values of the figure of merit, as shown in Tables II and III. Additional confidence that valid, high resolution information is indeed really present in the images is provided by the fact that optical diffraction

patterns that are overexposed at lower resolution show faint, spotty rings out to the resolution of the (4, 0) reflection. These rings, illustrated in Fig. 6, while broad, are too sharp to be phase contrast rings from the amorphous carbon support film. We therefore conclude that they represent crystalline diffraction from a large number of small, mosaic domains, each of which is quite well preserved, but most of which are too small to provide a recognizable optical diffraction pattern of their own.

DISCUSSION

The filtered image of the negatively stained OmpC specimen, which is shown on Fig. 4 *a*, confirms that the structure of this membrane protein must be very similar to that of OmpF. A strong similarity between these two proteins is expected since they have similar biochemical characteristics and physiological functions. Furthermore, although we have used lipid A (the core structure of outer

TABLE II
VALUES OF THE AMPLITUDE AND PHASE OBTAINED FROM SYMMETRY RELATED REFLECTIONS

H	K	Bragg spacing Å	Type I				Type II			
			Phase	Amplitude	$\frac{A-\mu^*}{\sigma}$	m‡	Phase	Amplitude	$\frac{A-\mu}{\sigma}$	m
$\frac{1}{2}$	1		102	62,500	3.6	0.95	59	22,700	0.3	0.57
$\frac{2}{2}$	$\frac{1}{2}$	39.0	99	69,100	3.8	0.95	113	45,900	2.2	0.88
1	$\frac{2}{2}$		124	74,500	4.4	1.00	160	58,100	3.9	0.95
$\frac{2}{2}$	0		40	69,700	5.1	1.00	107	59,300	3.7	0.95
$\frac{2}{2}$	$\frac{2}{2}$	33.8	106	71,300	4.2	1.00	126	61,600	4.6	1.00
0	$\frac{2}{2}$		106	40,600	2.0	0.86	137	47,300	2.9	0.92
$\frac{1}{3}$	2		73	63,500	3.9	0.95	56	45,600	3.0	0.93
$\frac{1}{3}$	$\frac{1}{3}$	25.5	113	42,700	1.4	0.78	82	34,500	1.8	0.84
2	$\frac{1}{3}$		73	35,700	2.3	0.88	64	46,800	2.8	0.92
$\frac{2}{3}$	1		66	78,900	5.3	1.00	47	105,200	8.2	1.00
$\frac{2}{3}$	$\frac{2}{3}$	25.5	46	70,100	3.1	0.93	99	102,000	9.9	1.00
1	$\frac{2}{3}$		19	46,300	2.5	0.90	72	102,000	8.3	1.00
$\frac{3}{3}$	0		101	32,000	1.6	0.81	73	33,800	2.1	0.87
$\frac{3}{3}$	$\frac{3}{3}$	22.5	93	24,600	1.4	0.78	128	22,000	0.8	0.68
0	$\frac{3}{3}$		139	21,600	0.6	0.64	162	27,700	1.1	0.73
$\frac{2}{4}$	2		15	15,500	0.3	0.57	75	24,600	1.4	0.78
$\frac{2}{4}$	$\frac{2}{4}$	19.5	61	30,000	2.3	0.88	23	18,500	0.5	0.62
2	$\frac{2}{4}$		329	42,300	2.3	0.88	11	30,000	2.1	0.87
$\frac{1}{4}$	3						44	17,100	0.1	0.50
$\frac{1}{4}$	$\frac{1}{4}$	18.7	—	—	—	—	150	15,800	0.3	0.56
3	$\frac{1}{4}$						142	31,000	1.9	0.85
$\frac{3}{4}$	1		344	29,500	1.9	0.85				
$\frac{3}{4}$	$\frac{3}{4}$	18.7	301	28,600	1.5	0.79	—	—	—	—
1	$\frac{3}{4}$		349	21,200	0.3	0.57				
$\frac{4}{4}$	0		171	30,800	1.6	0.81	263	26,800	1.8	0.84
$\frac{4}{4}$	$\frac{4}{4}$	16.9	211	31,300	2.1	0.87	214	25,700	1.9	0.85
0	$\frac{4}{4}$		160	39,100	3.4	0.94	181	60,400	5.5	1.00
$\frac{2}{5}$	3		272	25,100	1.5	0.79				
$\frac{2}{5}$	$\frac{2}{5}$	15.5	323	33,800	2.5	0.90	—	—	—	—
3	$\frac{2}{5}$		300	20,300	0.9	0.70				
$\frac{3}{5}$	2						254	30,000	2.4	0.89
$\frac{3}{5}$	$\frac{3}{5}$	15.5	—	—	—	—	308	14,800	0.2	0.55
2	$\frac{3}{5}$						305	27,600	2.2	0.88
$\frac{5}{5}$	0		200	26,600	1.7	0.82	349	29,400	2.5	0.90
$\frac{5}{5}$	$\frac{5}{5}$	13.5	175	33,600	2.2	0.88	332	12,300	0.0	0.50
0	$\frac{5}{5}$		211	24,500	1.8	0.84	304	19,200	0.6	0.64
		rms		phase error	21.67°	rms	phase error	29.99°		

*A is the amplitude, μ and σ are the mean value and the standard deviation of the local background.
‡m is the figure of merit associated with each reflection order.

membrane lipopolysaccharide) to reconstitute our OmpC specimens, the unit cell dimensions, 67.5 Å in our studies, and the trimer packing within the unit cell are very similar to those obtained when OmpF is reconstituted with phospholipid, at a low molar ratio of lipid to protein (Dorset et al., 1983).

The filtered images of frozen hydrated specimens of OmpC extend what can be learned beyond that which is seen in negatively stained specimens by showing, for the first time, the molecular envelope of the protein, projected within the plane of the membrane. The approximate molecular shape, the points of protein-protein contacts within trimers and between trimers, and a conspicuous low-density feature at a threefold symmetry axis are significant features of these images (Fig. 5). The low-density feature at the threefold axis undoubtedly represents a region of lipid bilayer, since the projected density of lipid A is much lower than that of protein, even when the presence of the carbohydrate at the polar surface is taken into consideration. Note that the area of this negatively contoured region of the map is sufficient to exactly accommodate a bilayer with three lipid A molecules (i.e., 15 acyl chains) on each side of the bilayer, thereby suggesting that the acyl chains could be crystallographically ordered at this threefold position in the lattice. The Type I and Type II images shown in Fig. 5 have a similar distribution of protein, aqueous channels, and lipid domain. However, details of the molecular shape of the protein as well as the orientation of each protein trimer are slightly different.

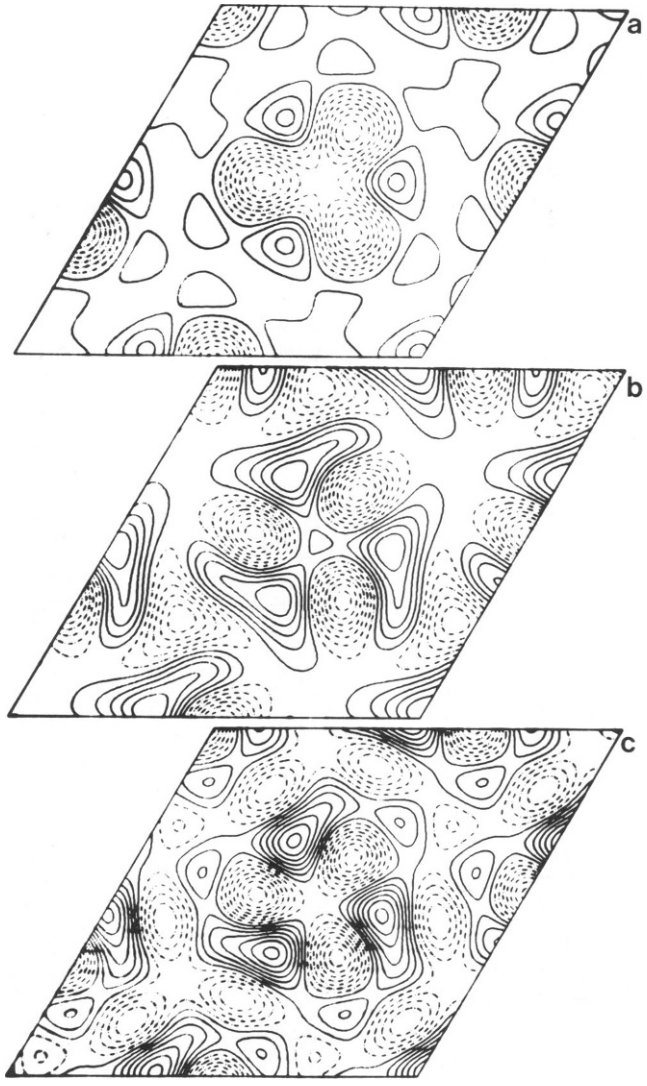

FIGURE 4 Computer filtered images of (*a*) negatively stained OmpC specimen, (*b*) Type I frozen-hydrated OmpC specimen, and (*c*) Type II frozen-hydrated OmpC specimen. Positive contours represent the protein domain in all three images and negative contours represent (*a*) the stain occupied region, (*b*), and (*c*) aqueous channels and the lipid domain. Fourier coefficients of the highest reflection order incorporated in these filtered images correspond to a resolution of 25.5 Å.

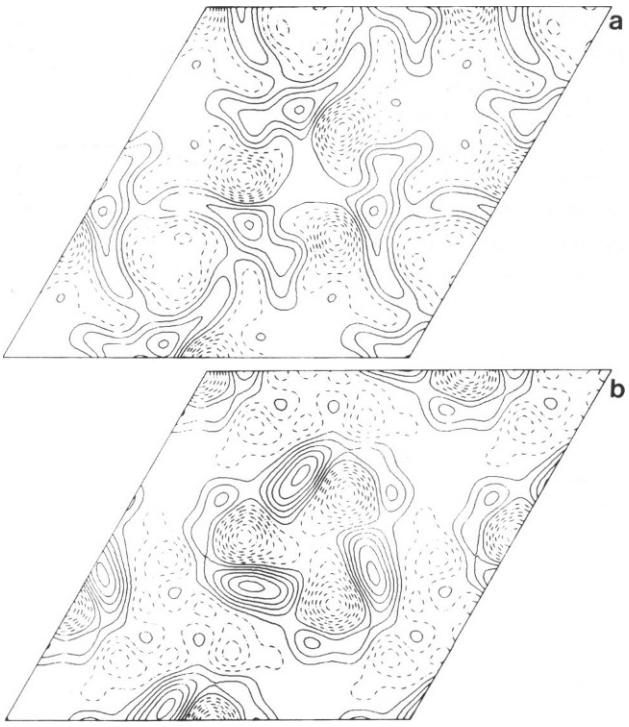

FIGURE 5 Computer filtered, high resolution images of frozen-hydrated OmpC specimens. The Fourier coefficients incorporated in these images are shown in Table III. (*a*) Type I image and (*b*) Type II image.

We first suspected that the Type I image, Fig. 5 *a*, was actually a twinned version of the Type II image, Fig. 5 *b*. If this were true, it should be possible to represent the Fourier coefficients for the Type I image as a linear combination of the Fourier coefficients of two versions of the Type II image, each in a different, twinned orientation. However, when all possible superpositions were tried, there was no good agreement that could be obtained between the Type I image and twins that were synthesized from the Type II image.

Substantial improvements will have to be made in the

TABLE III
SYMMETRIZED FOURIER COEFFICIENTS AND COMPOSITE m VALUES OBTAINED BY USING THE p3-RELATED DATA SHOWN IN TABLE II

H	K	Type I			Type II		
		Weighted amplitude	Composite phase	Composite figure of merit	Weighted amplitude	Composite phase	Composite figure of merit
$\frac{1}{2}$ 1	1 $\frac{1}{2}$	67,400	109	0.98	35,300	120	0.78
$\frac{2}{2}$ 0	0 $\frac{2}{2}$	52,300	84	0.85	55,100	123	0.98
$\frac{1}{3}$ 2	2 $\frac{1}{3}$	45,500	85	0.95	41,700	67	0.98
$\frac{2}{3}$ 1	1 $\frac{2}{3}$	61,700	45	0.94	95,900	73	0.93
$\frac{3}{3}$ 0	0 $\frac{3}{3}$	24,800	109	0.94	22,400	118	0.79
$\frac{2}{4}$ 2	$\frac{2}{2}$ 4	23,900	15	0.77	22,000	36	0.88
$\frac{1}{4}$ 3	3 $\frac{1}{4}$	—	—	—	16,700	125	0.73
$\frac{3}{4}$ 1	1 $\frac{3}{4}$	25,100	330	0.93	—	—	—
$\frac{4}{4}$ 0	0 $\frac{4}{4}$	31,600	180	0.93	32,300	216	0.83
$\frac{2}{5}$ 3	3 $\frac{2}{5}$	25,100	300	0.93	—	—	—
$\frac{3}{5}$ 2	2 $\frac{3}{5}$	—	—	—	23,000	286	0.90
$\frac{5}{5}$ 0	0 $\frac{5}{5}$	27,200	165	0.96	20,500	331	0.94

size of individual, coherent crystalline areas of membrane before it will be possible to extend the image resolution to values better than 10 Å. In addition, data collection for a three-dimensional reconstruction of frozen hydrated specimens will be quite difficult with the present type of specimen. This is true not only because of the small coherent patch size, but also because of the presence of more than one crystal polymorph. Although the two crystal forms observed in the present work are readily distinguishable from one another in the equatorial plane, this could be less true for tilted specimens, a fact that would seriously confound the task of merging three-dimensional data.

The factors that limit the size of coherently ordered crystalline domains are not known at present. Traces of bound lipopolysaccharide are thought to interfere with the formation of crystalline arrays; different lattice packing of trimers (reflected in different lattice constants and even different plane-group symmetry) can occur, depending upon the local lipid-to-protein ratio (Yamada and Mizushima, 1980); and the possible fluctuation of individual trimers between open and closed conformational states may result in illegitimate lattice bonding between adjacent unit cells, which would interfere with the formation of large coherent arrays. All of these potential difficulties,

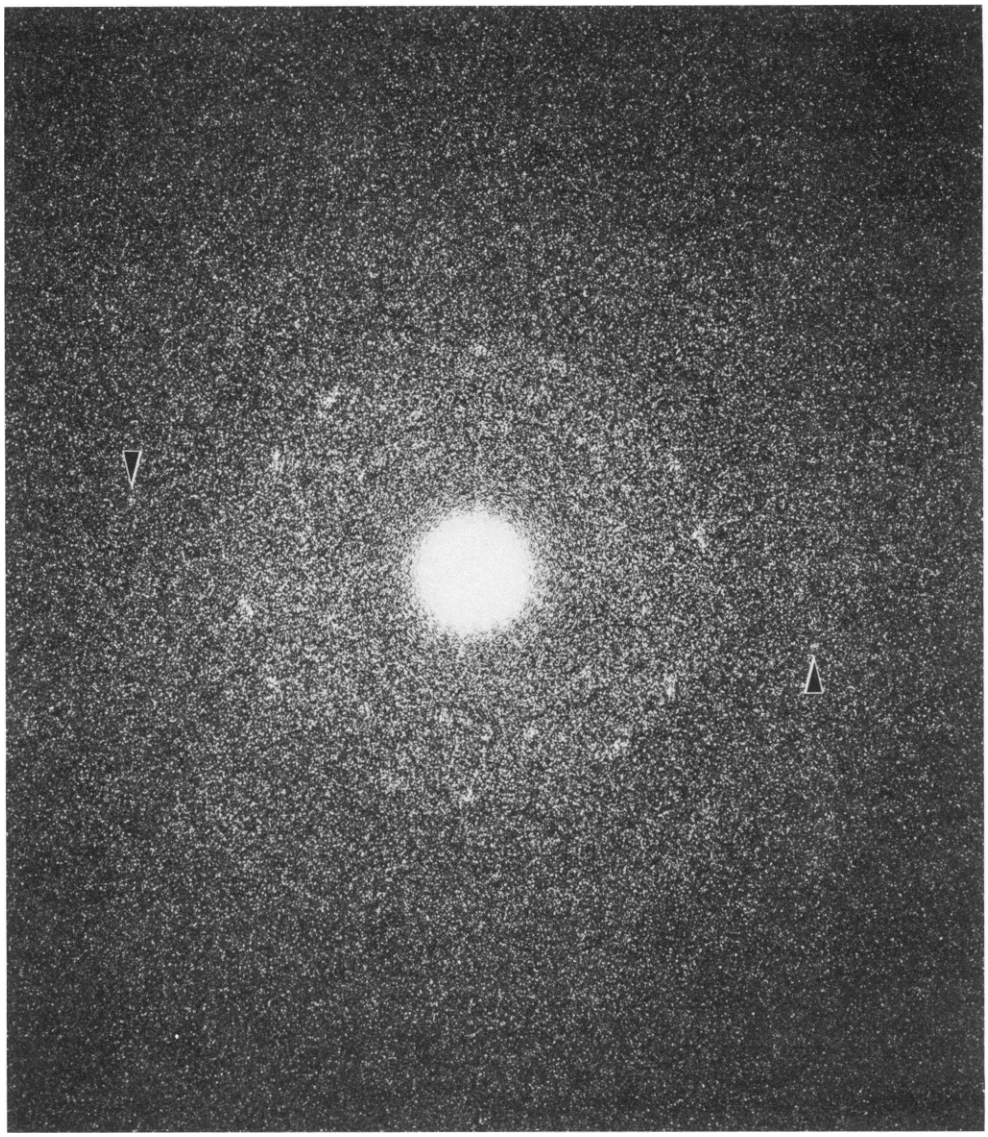

FIGURE 6 An overexposed print of the optical diffraction pattern shown in Fig. 3 *a*. The (4,0) spot, identified by the arrow is visible in the pattern. The feature corresponds to a resolution of 16.8 Å.

and quite possibly others as well, will have to be overcome before a significant degree of further progress can be made on the structure of this pore-forming protein.

We are grateful to Dr. Ken Downing for valuable discussion on the evaluation of figure of merit and to Dr. Hisami Yamada for reconstituted specimens.

This work was supported in part by postdoctoral training grant HLO7499 from the National Institutes of Health (to C.-F. Chang) and by grant GM23325 also from NIH (to R. M. Glaeser).

Received for publication 23 August 1984 and in final form 12 December 1984.

REFERENCES

Blow, D. M., and F. H. C. Crick. 1959. The treatment of errors in the isomorphous replacement method. *Acta Crystallogr.* 12:794-802.

Chang, C.-F., T. Ohno, and R. M. Glaeser. 1985. The fatty acid monolayer technique for preparing frozen-hydrated specimens. *J. Electron Microsc. Technique.* 2: 59–65.

Chen, R., C. Kramer, W. Schmidmayr, U. Chen-Schmeisser, and U. Henning. 1982. Primary structure of major outer-membrane protein I (OmpF protein, porin) of *Escherichia coli* B/2. *Biochem. J.* 203:33–43.

Dorset, D. L., A. Engel, M. Haner, A. Massalski, and J. P. Rosenbusch. 1983. Two-dimensional crystal packing of matrix porin: a channel forming protein in *E. coli* outer membranes. *J. Mol. Biol.* 165:701–710.

Dorset, D. L., A. Engel, A. Massalski, and J. P. Rosenbusch. 1984. Three dimensional structure of a membrane pore. Electron microscopical analysis of *Escherichia coli* outer membrane matrix porin. *Biophys. J.* 45:128–129.

Downing, K. D., and R. M. Glaeser. 1984. Simplified treatment of statistical errors in electron crystallography. *In* Electron Microscopy. Á. Csanády, P. Röhlich, D. Szabó, editors. The Programme Committee

of the 8th European Congress on Electron Microscopy (Budapest). 2: 1341–1342.

Galanos, C., E. Th. Rietschel, O. Luderitz, and O. Westphal. 1971. Interaction of lipopolysaccharides and lipid A with complement. *Eur. J. Biochem.* 19:143–152.

Garavito, R. M., J. A. Jenkins, J. H. Jansonius, R. Karlsson, and J. P. Rosenbusch. 1983. X-ray diffraction of matrix protein. An integral membrane protein from *E. coli* outer membrane. *J. Mol. Biol.* 164:313–327.

Grano, D. A., C.-F. Chang, and R. M. Glaeser. 1982. Structural investigations of the pore-forming OmpC protein from *E. coli*. Proc. Electron Microsc. Soc. *40th*. 90–91.

Hayward, S. B., and R. M. Glaeser. 1980. High resolution cold stage for the JEOL 100B and 100C electron microscopes. *Ultramicroscopy.* 5:3–8.

Hayward, S. B., and R. M. Stroud. 1981. Projected structure of purple membrane determined to 3.7 Å resolution by low temperature electron microscopy. *J. Mol. Biol.* 151:491–517.

Hayward, S. B., D. A. Grano, R. M. Glaeser, and K. A. Fisher. 1978. Molecular orientation of bacteriorhodopsin within the purple membrane of *Halobacterium halobium*. *Proc. Natl. Acad. Sci. USA.* 75:4320–4324.

Inokuchi, K., N. Mutoh, S. Matsuyama, and S. Mizushima. 1982. Primary structure of the OmpF gene that codes for a major outer membrane protein of *Escherichia coli* K-12. *Nucleic Acids Res.* 10:6957–6968.

Kawaji, H., T. Mizuno, and S. Mizushima. 1979. Influence of molecular size and osmolarity of sugars and dextrans on the synthesis of outer membrane proteins 0-8 and 0-9 of *Escherichia coli* K-12. *J. Bacteriol.* 140:843–847.

Nakae, T. 1976. Identification of the outer membrane protein of *E. coli* that produces transmembrane channels in reconstituted vesicle membranes. *Biochem. Biophys. Res. Commun.* 71:877–884.

Nakamura, K., D. N. Ostrovsky, T. Miyazawa, and S. Mizushima. 1974. Infrared spectra of outer and cytoplasmic membrane of *Escherichia coli*. *Biochim. Biophys. Acta.* 332:329–335.

Nikaido, H., and E. Y. Rosenberg. 1983. Porin channels in *Escherichia coli:* studies with liposomes reconstituted from purified proteins. *J. Bacteriol.* 153:241–252.

Rosenbusch, J. P. 1974. Characterization of the major envelope protein from *Escherichia coli*. *J. Biol. Chem.* 249:8019–8029.

Schindler, H., and J. P. Rosenbusch. 1978. Matrix protein from *Escherichia coli* outer membrane forms voltage controlled channels in lipid bilayers. *Proc. Natl. Acad. Sci. USA.* 75:3751–3755.

Schindler, H., and J. P. Rosenbusch. 1981. Matrix protein in planar membranes: Clusters of channels in a native environment and their functional reassembly. *Proc. Natl. Acad. Sci. USA.* 78:2302–2306.

Steven, A. C., B. ten Heggeler, R. Muller, J. Kistler, and J. P. Rosenbusch. 1977. Ultrastructure of a periodic protein layer in the outer membrane of *Escherichia coli*. *J. Cell Biol.* 72:292–301.

Van Alphen W., and B. Lugtenberg. 1977. Influence of osmolarity of the growth medium on the outer membrane protein pattern of *Escherichia coli*. *J. Bacteriol.* 131:623–630.

Williams, R. C. 1981. Morphology of bovine fibrinogen monomers and fibrin oligomers. *J. Mol. Biol.* 150:399–408.

Yamada, H., and S. Mizushima. 1978. Reconstitution of an ordered structure from major outer membrane constituents and lipoprotein-bearing peptidoglycan sacculus of *Escherichia coli*. *J. Bacteriol.* 135:1024–1031.

Yamada, H., and S. Mizushima. 1980. Interaction between major outer membrane protein (0-8) and lipopolysaccharide in *Escherichia coli* K-12. *Eur. J. Biochem.* 103:209–218.